Air spark-like plasma source for antimicrobial NO_x generation

2014 J. Phys. D: Appl. Phys. 47 505202

(http://iopscience.iop.org/0022-3727/47/50/505202)

IOP Publishing Journal of Physics D: Applied Physics
J. Phys. D: Appl. Phys. **47** (2014) 505202 (10pp) doi:10.1088/0022-3727/47/50/505202

Air spark-like plasma source for antimicrobial NO_x generation

M J Pavlovich[1], T Ono[2], C Galleher[1], B Curtis[1], D S Clark[1], Z Machala[3] and D B Graves[1]

[1] Department of Chemical and Biomolecular Engineering, University of California, Berkeley, CA 94720, USA
[2] Department of Electrical Engineering, Tokyo Institute of Technology, Tokyo, Japan
[3] Faculty of Mathematics, Physics and Informatics, Comenius University, 84248 Bratislava, Slovakia

E-mail: graves@berkeley.edu

Received 29 August 2014, revised 5 October 2014
Accepted for publication 21 October 2014
Published 25 November 2014

Abstract

We demonstrate and analyse the generation of nitrogen oxides and their antimicrobial efficacy using atmospheric air spark-like plasmas. Spark-like discharges in air in a 1 L confined volume are shown to generate NO_x at an initial rate of about 1.5×10^{16} NO_x molecules/J dissipated in the plasma. Such a discharge operating in this confined volume generates on the order of 6000 ppm NO_x in 10 min. Around 90% of the NO_x is in the form of NO_2 after several minutes of operation in the confined volume, suggesting that NO_2 is the dominant antimicrobial component. The strong antimicrobial action of the NO_x mixture after several minutes of plasma operation is demonstrated by measuring rates of *E. coli* disinfection on surfaces and in water exposed to the NO_x mixture. Some possible applications of plasma generation of NO_x (perhaps followed by dissolution in water) include disinfection of surfaces, skin or wound antisepsis, and sterilization of medical instruments at or near room temperature.

Keywords: air plasma, nitrogen oxides, disinfection, atmospheric-pressure plasma, spark discharges

(Some figures may appear in colour only in the online journal)

1. Introduction

The recent literature on atmospheric plasma applications in surface and water disinfection is growing rapidly, and the fact that air plasmas generate antimicrobial conditions and chemical species is now well known [1, 2]. Air plasma using dielectric barrier discharges (DBDs), gliding arcs, and similar devices have been shown by various groups to generate strongly antimicrobial components, capable of rapidly disinfecting adjacent surfaces and liquids [3–7]. If operated near water, these discharges can create what has been termed 'plasma-activated water'. Chemical analysis of the gas phase near these discharges has revealed stable gas phase species such as ozone (O_3); nitric (HNO_3) and nitrous (HNO_2) acids; and various nitrogen oxides such as nitric oxide (NO), nitrogen dioxide (NO_2) and nitrous oxide (N_2O). NO, NO_2, O_3, and hydrogen peroxide (H_2O_2) will dissolve directly from the gas phase into adjacent water, although their aqueous solubilities differ markedly. Depending on the solution pH, the nitrate (NO_3^-) and nitrite (NO_2^-) anions will be present in the water adjacent to the air plasma. Nitric acid is a very strong acid and will be nearly fully ionized to form NO_3^- in aqueous solutions that are not buffered. Nitrous acid has a pKa of about 3.4, so it may or may not be fully ionized into nitrite, depending on the pH, as established, for example, by the concentration of HNO_3.

Other chemical species are no doubt present in water adjacent to air plasma, including N_xO_y compounds and their corresponding acids [8]. One that has received much attention recently in the context of plasma-activated water is peroxynitrite ($ONOO^-$) or peroxynitrous acid (ONOOH) [6, 9, 10]. A well-established method to generate peroxynitrite is to mix aqueous solutions of acidified H_2O_2 with NO_2^- [11, 12]. Both of these species are known to be created in air plasma, so it seems likely that $ONOO^-$ (or ONOOH) is also generated in water exposed to air plasma. At room temperature and

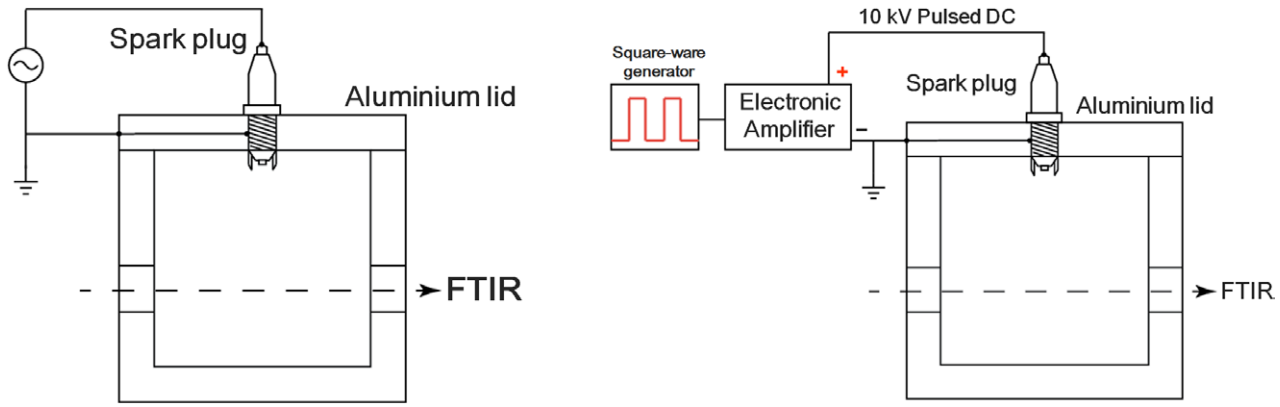

Figure 1. Sketch of the 1 L volume 'NO_x Box' showing the acrylic body, grounded aluminum top, conventional automotive spark plug, and power supply. FTIR absorption was used to measure gas phase species evolving during operation and afterglow of the spark-like plasma. Left: quasi-sinusoidal ac waveform, right: square-wave dc waveform.

non-basic pH, aqueous peroxynitrite has a relatively short lifetime, on the order of seconds. However, at −80 °C and strongly basic pH, it can be maintained for up to one year in storage [11]. The complex chemistry of air plasmas and the associated plasma–water chemistry are areas of active research, and further investigation will be needed to fully understand these systems; coupled air plasma and chemical kinetic models and corresponding gas phase and water chemistry studies are beginning to appear in the literature [12–16].

The primary purpose of this article is to describe a class of plasma devices using spark-like discharges and operating in air, sometimes using small amounts of water, which can be exploited for applications including biocides, disinfectants, sterilization, and antisepsis, among others. We use the term 'spark-like' plasma because a spark discharge is generally considered to be a fully transient discharge [17]. In our discharges, however, there appears to be significant quasi-glow like character. This spark-to-glow transition has been studied previously [18, 19], and dc atmospheric-pressure air glow discharges have been discussed in the literature [20–22]. Detailed investigations of spark and glow discharges have been made, for example, in studies of combustion for automotive engines [23].

The important reactive species created in the air spark-like plasmas are primarily nitrogen dioxide and nitric oxide. The literature on NO and NO_2 is extensive and certainly cannot be comprehensively summarized here [24]. Briefly, NO is one of the physiologically important classes of molecules referred to as 'reactive nitrogen species' (RNS) [25, 26]. NO_2 is an important air pollutant and, along with NO, plays a key role in atmospheric chemistry [27]. The nitrite anion, especially under acidic conditions in aqueous solution, has received considerable attention in the last several decades for its direct and indirect physiological roles, connection to NO in the body, therapeutic action, and use as a disinfectant, among other reasons [28, 29]. It is known that NO_x generation is favoured by higher-temperature air plasmas, so we chose to explore their generation using air spark-like discharges [30]. Furthermore, we have characterized these species in disinfecting adjacent surfaces and in forming a strongly antimicrobial aqueous solution [3, 31, 32].

The importance of NO generated in air plasma for wound sterilization and healing, and related plasma therapeutic applications, has been noted by others, but the potentially key role of NO_2 seems not to have been strongly emphasized in the previous air plasma literature [33, 34]. Kim *et al* reported the use of a microwave plasma operating at atmospheric pressure in flowing O_2/N_2 mixtures to create NO_x, mostly in the form of NO_2 [35]. These authors also summarize results from various papers reporting that the production rate of NO_x molecules from spark discharges typically ranges from the order of 10^{16}–10^{17} NO_x molecules generated/J dissipated in the spark. We return to this figure later in the article to show that it is close to our results.

In the present article, we describe a device that utilizes spark-like electrical discharges in ambient air to create various potentially useful chemical species such nitrogen oxides, which in some cases are mixed into water. We describe the devices, power supplies, and electrode designs, along with their basic discharge physics and chemistry. FTIR spectroscopy is used to characterize the gas-phase composition from the plasma devices, and liquid phase UV-Vis absorption measurements are made for nitrate (NO_3^-), and nitrite (NO_2^-). Next, we characterize the effects of these species for inactivating *Escherichia coli* bacteria either dried on metal surfaces or dissolved in water. Finally, we detail some envisioned applications and offer a vision of how this technology might develop in the future.

2. Experimental

2.1. NO_x Box with spark-like discharge

The reactor used in this study was an acrylic chamber measuring 10 × 10 × 10 cm (or 1 L in volume) with an automobile spark plug (Bosch Platinum 4417) mounted on the top, and two infrared-transparent windows (CaF_2, Edmund Optics) on parallel sides. A schematic of the chamber is shown in figure 1. This reactor was filled with air at room temperature, atmospheric pressure, and ambient humidity, and it was used to enclose and measure the chemical species produced by the spark-like air plasma, consisting primarily of

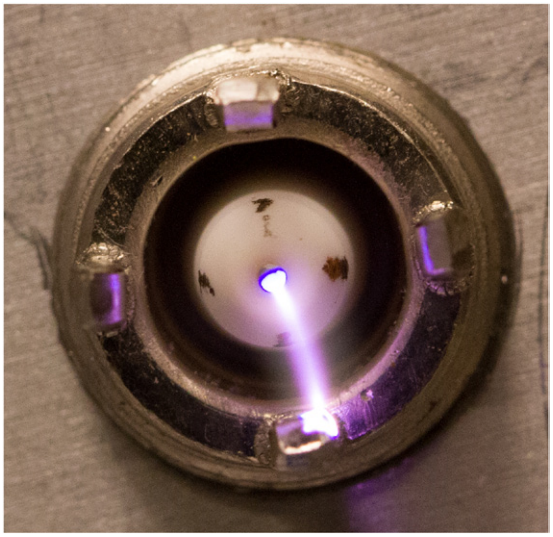

Figure 2. Photo of the spark-like discharge created using a spark plug altered to allow the spark to form between the centre powered electrode and the grounded posts. The spark length is about 5 mm (photo courtesy of Steve Graves).

nitrogen oxides (NO_x). We term this chamber the 'NO_x Box'. The NO_x Box was operated as a batch reactor, with the gas present at the beginning of treatment sealed inside the box for the duration of the operation. Following each operation, the box was opened and vented inside a fume hood and purged with nitrogen before refilling with ambient air for the next operation. The spark plug was powered by either the ac or pulsed dc discharge described below. The conventional spark plug was slightly modified to increase the inter-electrode gap distance to 5 mm. This increase in spark length significantly increased the rate of NO_x generation, presumably by increasing the gas temperature in the spark. A photograph of a typical spark-like discharge is shown in figure 2. The relatively high-temperature plasma created in the repetitive spark-like discharge resulted in significant production of NO_x that diffused throughout the box volume over periods of minutes to tens of minutes. Metal discs with *E. coli* bacteria dried on the surface, or vials containing bacterial suspensions in water, were placed on the bottom of the box and treated for specific times. The distance from the plasma discharge to the treated samples was approximately 9 cm. Corresponding sets of the time evolution of gaseous NO_x concentrations were measured via *in-situ*, real-time FTIR analysis.

To generate the spark-like discharge, we used a high-voltage power supply consisting of a high-voltage amplifier (Trek model 10/40A) combined with a synthesized function generator (Protek 31 MHz 9301). In one configuration, this power supply generates a quasi-sinusoidal ac waveform with 6 kV peak-to-peak amplitude and 5 kHz frequency. Typical operation of the NO_x Box spark plug using a quasi-sinusoidal ac waveform resulted in a power input to the spark of about 35 W.

In addition, we ran various spark-glow hybrid modes on the spark plug in the NO_x Box to investigate how the discharge affects the gas chemistry. The time duration of the glow discharge was manipulated by changing the square wave voltage duty cycle. Frequency was fixed at 1 kHz, and the duty cycle was changed from 2 to 100%, corresponding to glow discharge time 50–1000 μs. The voltage was measured in all configurations by a high-voltage probe (Tektronix P6015A) and a 200 MHz digital oscilloscope (Tektronix 2024C). Figure 3 compares the time evolutions of the voltage and current waveforms used to generate the spark-like discharges. The hybrid spark-glow character can be seen most clearly in the voltage waveform of the square-wave dc function, illustrated in figure 3, in which a relatively stable dc current occurs over a large part of each discharge cycle after a well-defined spark breakdown. Power was calculated by numerically integrating the product of the voltage and current waveforms and multiplying by the frequency (1 kHz).

2.2. FTIR spectroscopy

Fourier transform infrared (FTIR) spectroscopy was performed as an *in-situ* gas product diagnostic in the NO_x Box described above. The NO_x Box was placed inside an infrared spectrometer (DIGILAB Excalibur Series, MOD. FTS 3000) so that the infrared beam passed through calcium fluoride windows placed in the walls of the acrylic chamber. The FTIR beam passed through the box approximately 8 cm below the spark plug with the discharge, and we assume relatively uniform diffusion of plasma-generated NO_x species throughout the box. Absorption FTIR spectra were recorded over time since the plasma was ignited and later switched off, typically after 10 min. The wavenumber resolution of the measurements was 1 cm^{-1}, and between 20 and 200 scans were typically averaged to create each spectrum. The time resolution of the measurements was between 30 s and 2 min. The following vibrational bands were used as diagnostics for the presence of reactive species: O_3 at 1055 cm^{-1}; NO at 1900 cm^{-1}; NO_2 at 1630 and 2916 cm^{-1}; N_2O_4 at 1261, 1763, and 2976 cm^{-1} [36, 37]; and HNO_3 at 1325 and 1718 cm^{-1}. The absolute concentrations of NO and NO_2 were estimated by fitting the measured FTIR spectra to spectra simulated using parameters in the HITRAN database (http://hitran.iao.ru/). To generate simulated standard spectra, we used a wavenumber range of 500–4000 cm^{-1}, a wavenumber computational step of 0.01 cm^{-1}, an optical path of 0.1 m (corresponding to the window-to-window width of the NO_x Box), an assumed Gaussian apparatus function, and an apparatus resolution of 1 cm^{-1}. The species concentration was adjusted to find the best fit with the experimentally measured spectra. For NO, the relationship between absorbance and concentration remained linear over the range tested. For NO_2, we observed significant nonlinearity in the absorbance/concentration relationship above concentrations of 1000 ppm when using the strong band at 1630 cm^{-1}. The phenomenon of non-linearity in gas-phase FTIR spectroscopy at high gaseous concentrations is known and has been discussed in the literature [38]. Therefore, we confirmed the gaseous NO_2 concentrations determined via FTIR with visible absorption at 404 nm. NO_2 concentrations determined by visible absorption showed good agreement with concentrations determined by the weak 2916 cm^{-1} vibrational band in FTIR, so all NO_2

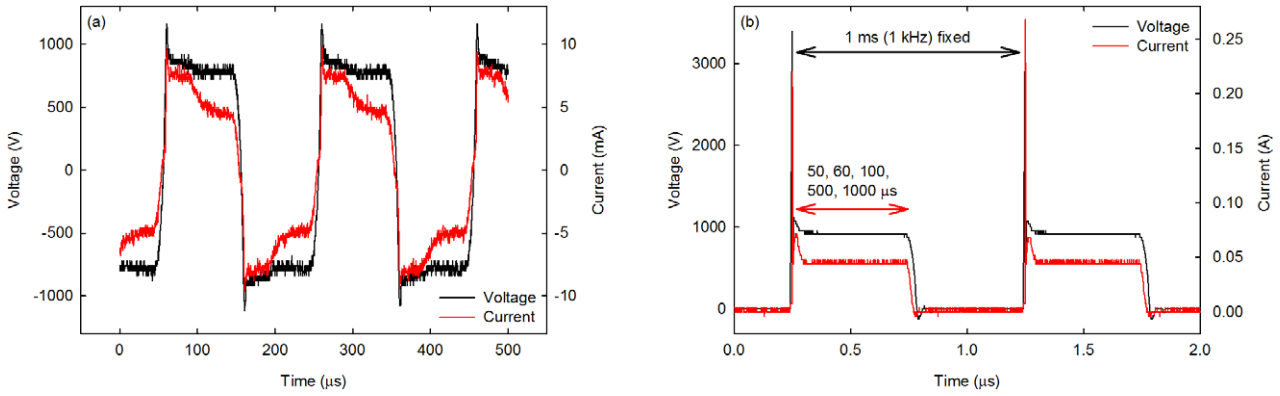

Figure 3. (*a*) Quasi-sinusoidal ac waveform, (*b*) square-wave dc waveform.

concentrations reported were determined by fitting FTIR absorbance at 2916 cm^{-1}.

2.3. Aqueous phase measurements

Aqueous nitrate and nitrite concentrations were measured via UV-visible absorbance spectroscopy (Molecular Devices, Spectramax M2) [31]. Spectra were recorded between 230 and 430 nm using Nanopure water as a reference blank. Concentration standards were generated with sodium nitrate and sodium nitrite at pH 2, and least-squares regression was used to fit experimentally measured spectra to the standards. Absorbance maxima were observed near 300 nm (nitrate) and 360 nm (nitrite).

2.4. Evaluation of bactericidal effects on E. coli

E. coli K12 was cultured and prepared as described previously [3, 31]. Bacteria were grown in lysogeny broth (LB) medium to OD_{600} corresponding to approximately 10^8 colony-forming units per ml (cfu ml^{-1}). For aqueous disinfection by NO_x, cells were diluted by a factor of 100 and suspended in sterile physiological saline (0.9% NaCl, Sigma). 150 μl of the bacterial suspension was transferred to a glass vial and placed inside the NO_x Box for plasma treatment. Following plasma treatment, the suspension was immediately diluted by serial dilutions up to a factor of 10^5 and plated on LB agar. Plates were incubated overnight at 37 °C, and colonies were counted to determine the number of viable cells.

For the surface disinfection experiments, suspensions of *E. coli* were pelleted from 100 μl aliquots by centrifugation at 5000 rpm. *E. coli* bacteria were dried on stainless steel discs in preparation for exposure to plasma, and the steel discs were stored in a bath of 70% ethanol to prevent contamination prior to seeding with bacteria. Prior to adding bacteria to the discs, the discs were washed with sterile water that was allowed to evaporate completely from the surface of the disc. To seed the discs with bacteria, pellets of *E. coli* were spread across stainless steel discs with a plastic inoculating loop. The discs were allowed to dry in a sterile environment until the surface of the discs was no longer visibly wet and additional drying time did not result in any change in the appearance of the surface, generally approximately 1 h. This drying procedure did not significantly affect the bacterial viability. Once the surface was dry, the steel discs were placed inside the NO_x Box for plasma treatment. Following treatment, the discs were immediately immersed in 10 ml of phosphate buffer saline (PBS) and vortexed for 10 min to elute the bacteria from the surface. Then, the bacteria-rich elution was diluted and plated on agar as described above.

The antibacterial effect of each treatment was determined by calculating the log reduction, $\log(N_0/N)$, where N_0 is the number of viable cells present in an untreated sample, and N is the number of cells that remained viable following treatment. N_0 fluctuated by approximately a factor of 5; possible explanations for this fluctuation include slight day-to-day differences in the initial cell culture density as well as variation in the efficiency of eluting the bacteria from the untreated samples. The maximum log reduction that can be calculated by this method was approximately 4 for surface disinfection experiments and 5 for aqueous disinfection; in some of the cases reported below, the actual log reduction likely exceeded this measurable limit of 4 or 5 log reductions.

3. Results and discussion

Nitrogen oxides were generated by spark-like discharges in the closed 1 L volume of the NO_x Box. We measured NO_x production over the duration of the discharge operation, typically 1–20 min, and measured the concentration of NO_x for up to 1 h during the post-discharge period. The gas-phase concentrations of nitric oxide (NO) and nitrogen dioxide (NO_2) were measured as functions of time by FTIR. A typical FTIR spectrum is shown in figure 4, showing the presence of primarily NO_2, NO, N_2O_4, and HNO_3. Although it is possible that the presence of water vapor (i.e. humidity) could influence production of NO_x, the humidity in the ambient air we used fluctuated within a relatively narrow range (approximately 30–40%), and we did not observe a correlation between the humidity and the reactive species produced.

Both the quasi-sinusoidal ac and the square-wave dc functions were used to drive plasma generation. For the square-wave dc data, measurements were taken for various temporal contributions of the ‘glow-like’ and ‘spark-like’ character.

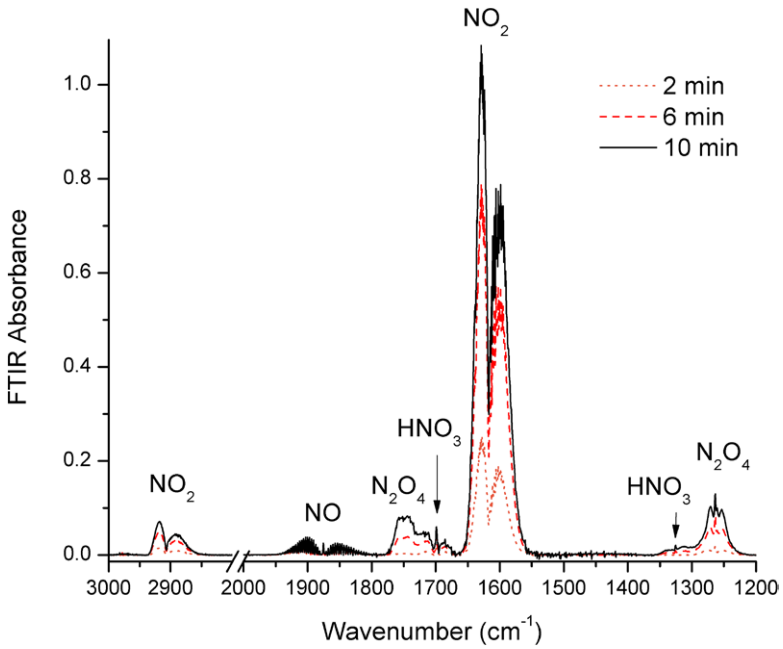

Figure 4. FTIR spectrum showing the temporal evolution of NO, NO_2, N_2O_4, and HNO_3 in the line of sight of the NO_x Box using the quasi-sinusoidal ac waveform.

Table 1. Summary of glow characteristics in the spark-like discharge generated by a square-wave dc discharge.

Glow discharge time (μs)	Glow percentage (%)	Total power (W)	Glow power (W)	Power density (kJ L^{-1})
1000	100	26.7	26.7	16.0
500	97.8	22.1	21.7	13.3
100	56.2	6.99	3.93	4.19
60	20.4	4.75	0.97	2.85
50	11.2	4.45	0.50	2.67

Glow percentage is defined as the percentage of the overall power consumption attributed to the 'glow-like' character.

Table 1 shows the glow percentages for which measurements were taken along with the corresponding glow discharge times and associated power consumptions.

The NO and NO_2 concentrations showed different behaviour as the glow power percentage increased. Figure 5 shows the relationship between glow discharge power percentage and NO_x concentration after 10 min of plasma treatment. The concentration of both NO and NO_2 increased with the glow power percentage up to 98%, where both NO and NO_2 reached a maximum concentration and did not increase significantly as the glow percentage was increased to 100%. In figures 5, 6, 8 and 9, the data shown are the mean of between two and five independent measurements, and the error bars represent standard deviations. The dotted lines used to connect the experimental data points serve as guides to visualize trends only.

Figure 6 shows plots of the spatially averaged NO and NO_2 concentrations normalized per discharge power versus elapsed time of spark-like discharge operation. Figure 6 shows that the optimum glow percentage (per Watt) was about 20% for NO and 56% for NO_2 production. This optimum is important to know when designing the optimum discharge regime for the antibacterial applications of the NO_x Box.

The time derivative of NO_x concentration in the volume is proportional to the net rate of NO_x generation. The initial (t = 0) rate of generation can be compared to previous estimates of NO_x production rates in terms of NO_x/J dissipated, as noted in the Introduction. Using the NO_2 ppm/W values in figure 7, we estimate that the initial generation rate using the ac quasi-sinusoidal wave is about 73 ppm/W/2 min, or equivalently about 0.61 ppm J^{-1}, with similar figures for the dc glow mode when the glow percentage was high. One part per million corresponds to about 2.5 × 10^{16} molecules in 1 L, assuming room temperature and atmospheric pressure in the box. Therefore, 0.61 ppm/J corresponds to about 1.5 × 10^{16} NO_x molecules created/J dissipated. 1.5 × 10^{16} NO_x molecules/J is in the range reported in the literature, as noted previously. The decrease in the net rate of generation that is observed as time increases is likely related to various gas-phase and perhaps surface loss processes, the detailed analysis of which will require further study.

An important point from figures 5 and 6 is that the gas phase composition is dominated by NO_2 by more than an order of magnitude over NO at longer times. However, it appears that within the first minute, NO concentration may be comparable to NO_2 concentration. NO is known to react with O_2 to form NO_2, and that NO_2 will react with itself to dimerize into N_2O_4; these reactions are sensitive to temperature and

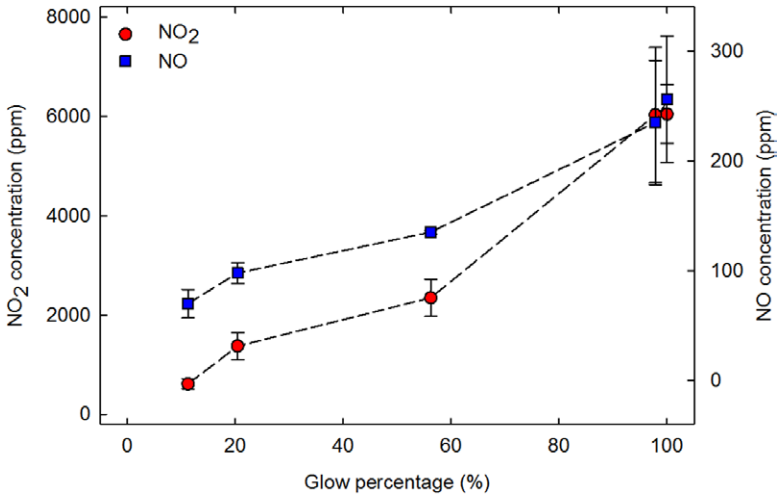

Figure 5. NO (blue squares) and NO_2 (red circles) concentrations after 10 min of plasma treatment as a function of the glow percentage.

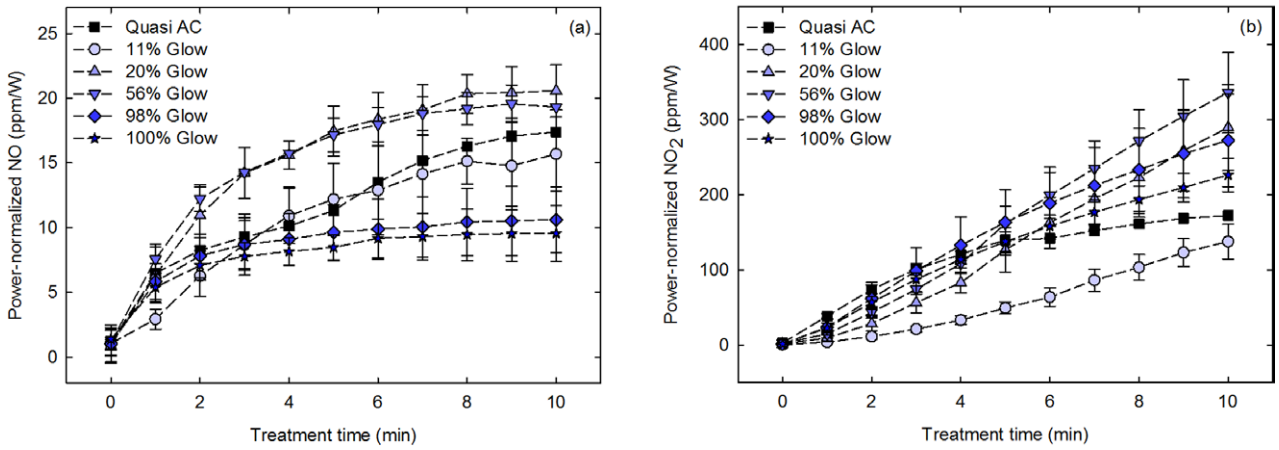

Figure 6. Temporal evolution of gas-phase (*a*) NO and (*b*) NO_2 power-normalized concentrations in the NO_x Box. Data are shown for both ac (black) and dc (blue) functions and various glow power percentages.

pressure. The plots in figure 6 can be rationalized in part by taking these reactions into account. Figure 7 demonstrates the relative evolution of NO, NO_2, N_2O_4 and other FTIR-detected species versus the elapsed time of the spark-like discharge operation up to 10 min (at glow percentage 56%) and during the post-discharge time (up to 30 min). It shows clearly that NO was the first product that quickly increased, followed by NO_2, N_2O_4, then HNO_2, and finally HNO_3. After the discharge was switched off, NO quickly decayed, followed by slower decay of NO_2, N_2O_4, and HNO_2. HNO_3 did not seem to decay within the investigated time at all. However, analysing the details of the NO_x chemistry in the volume is beyond the scope of this study. The problem is complicated by spatial gradients in the gas phase: gas mixing due to convective diffusion will certainly be important in the first few minutes, so this is a topic that will also require considerable further study.

The effect of treating water with the spark-like plasma generated NO_x was investigated by measuring aqueous concentrations of nitrite (NO_2^-) and nitrate (NO_3^-). Water treatment relied on the dissolution and diffusion of nitrogen oxides into the aqueous phase; solutions were not mixed to promote aqueous-phase mass transfer, and the relatively small water volume of 0.15 ml minimized transport limitations. Figure 8 shows the pH and the concentrations of aqueous nitrate and nitrite as a function of the solution's exposure time in the NO_x Box. The solution temperature increased by a few K after treatment. Although it was not possible to measure the solution temperature during treatment, assuming a heat of solution for nitric acid of $1.17 \times 10^5\,\mathrm{J\,mol^{-1}}$, we estimate that the solution temperature increased by approximately 2 K after 5 min of treatment. Solution heating could become more significant over extended periods of treatment, though we assume that the solution heating was not significant enough to affect the solution chemistry or antibacterial effect in this study.

We also determined the antibacterial effects in aqueous solution and on surfaces by exposing *E. coli* either suspended in physiological saline or dried on stainless steel discs to gaseous NO and NO_2. Bacterial log reductions for both aqueous suspensions and dry surfaces are shown as functions of time in figure 9.

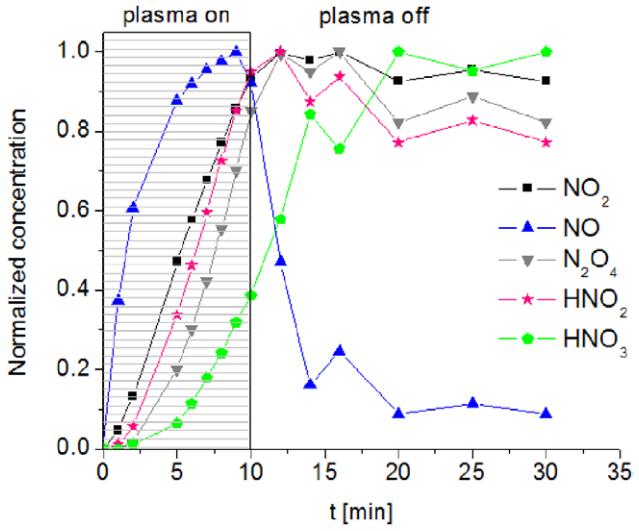

Figure 7. Relative evolution of the FTIR-detected species NO, NO_2, N_2O_4, HNO_2, and HNO_3 versus the elapsed time of the spark-like discharge operation up to 10 min (glow percentage 56%) and during the post-discharge time (up to 30 min). The concentration for each species is normalized to the maximum concentration of that species that was observed over the 30 min period. The maximum absolute concentrations were 3100 ppm at 16 min for NO_2, 140 ppm at 9 min for NO, and 80 ppm for HNO_3 at 30 min. The HITRAN database does not include information for N_2O_4 or HNO_2, so for those two species, we were only able to calculate relative (not absolute) concentrations.

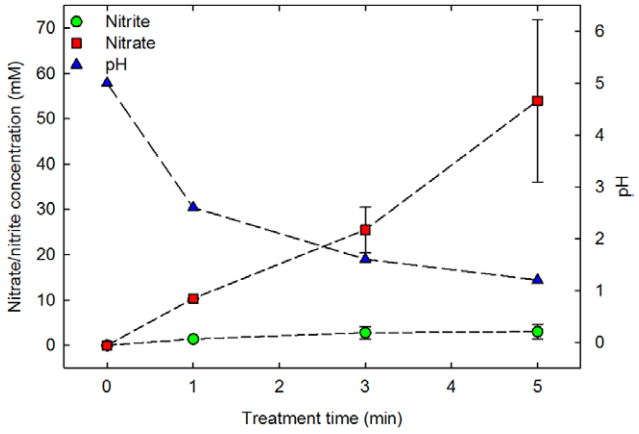

Figure 8. Temporal evolution of aqueous nitrite (circles) and nitrate (squares) concentrations and pH (triangles) in vials containing 150 μl of initially deionized water and placed in the NO_x Box, powered by the quasi-sinusoidal ac waveform. Note the differences in scale between nitrite and nitrate concentrations: nitrate dominates in the water. Note also that the measured pH corresponds approximately to the nitrate concentration assuming full ionization of nitric acid.

4. Discussion

Prior to plasma ignition, the gas inside the NO_x Box is ambient air, mainly consisting of N_2 and O_2, with some admixture of water vapor. NO_x species are produced and decomposed in air plasmas in a complex series of reactions that involve both thermal and non-thermal (i.e.

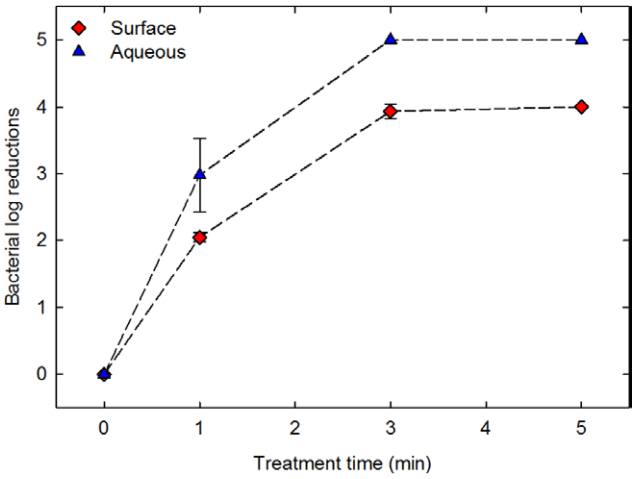

Figure 9. Temporal evolution of *E. coli* log reductions in aqueous saline solution (blue triangles) and on stainless steel surfaces (red diamonds) in the NO_x box powered by the quasi-sinusoidal ac waveform. Note that the log reductions at 5 min of treatment (5 logs for aqueous saline and 4 logs for stainless steel) correspond to the detection limits of our assay, meaning that none of the bacteria survived the treatment. Therefore, the actual log reductions for these conditions probably exceed what is shown here.

electron-impact driven) components. In addition, there are strong spatial gradients in the spark-glow plasma because the current channel contains both strong electron-impact and thermal processes. But when the species diffuse out of this relatively narrow channel, they cool rapidly, and chemical reactions outside the channel take place in the absence of plasma-induced reactions. The net effect is therefore a combination of multiple processes under vastly different conditions. The following discussion of likely mechanisms is therefore necessarily qualitative.

The thermal chemistry is driven by high gas temperatures in the (relatively narrow) plasma region of the spark/glow device. Spark-glow temperatures would probably be in the range of 2000 K or higher, but we did not attempt to measure gas temperature in this study [19–22, 39, 40]. The most widely accepted model of thermal NO_x production is the extended Zeldovich mechanism, in which the rate-limiting step is the reaction of N_2 with atomic oxygen O to form NO and N. The second reaction is the formation of NO from N and O_2, and the third reaction forming NO from N_2 requires the presence of OH [41, 42].

$$N_2 + O \rightarrow NO + N \quad (1)$$

$$N + O_2 \rightarrow NO + O \quad (2)$$

$$N_2 + OH \rightarrow NO + H \quad (3)$$

Note that the first two reactions (reactions 1 and 2) have analogues in the electron-impact reactions (listed below as reactions 9 and 10), but vibrationally/electronically excited N_2 and electronically excited N, written as N_2^* and N*, respectively, are thought to be the key intermediate species.

The electron-impact initiated chemistry is thoroughly documented in the literature [35, 43, 44]; the key reactions are listed below.

$$O_2 + e \rightarrow O + O + e \quad (4)$$

$$O_2 + e \rightarrow O + O^* + e \quad (5)$$

$$N_2 + e \rightarrow N_2^* + e \quad (6)$$

$$N_2^* + O_2 \rightarrow N_2 + O + O \quad (7)$$

$$O_2 + O + M \rightarrow O_3 + M \quad (8)$$

$$N_2^* + O \rightarrow NO + N^* \quad (9)$$

$$N^* + O_2 \rightarrow NO + O \quad (10)$$

$$N_2^* + NO \rightarrow N_2 + N + O \quad (11)$$

$$N + NO \rightarrow N_2 + O \quad (12)$$

$$O^* + NO \rightarrow N + O_2 \quad (13)$$

$$NO + O + M \rightarrow NO_2 + M \quad (14)$$

$$NO + O_3 \rightarrow NO_2 + O_2 \quad (15)$$

$$NO_2 + O \rightarrow NO + O_2 \quad (16)$$

$$NO_2 + M \leftrightarrow N_2O_4 + M \quad (17)$$

These reactions begin with the electron-impact dissociation of O_2 to O atoms (reactions 4 and 5) and the excitation of molecular nitrogen to various excited states of N_2^* (reaction 6). N_2^* is immediately de-excited (e.g. $N_2(C) \rightarrow N_2(B) + h\nu$ resulting in the N_2 2nd positive system emission associated with the typical blue appearance of air discharges) and quenched by O_2 molecules providing even more O atoms (reaction 7). Ozone is typically formed by the three-body collision of O_2 and O (reaction 8). NO is mainly generated through the collision of N_2^* or N_2 with O atoms resulting in excited N* or ground-state N atoms (reactions 9 and 1) which subsequently react with O_2 and form further NO and O (reactions 10 and 2). NO_2 is dominantly generated by a three-body collision between NO, O, and a third body (reaction 14) or by the oxidation of NO with O_3 (reaction 15). NO_2 will rapidly react with itself to dimerize into N_2O_4 (reaction 17), and this reaction is usually fast enough to be considered in equilibrium at room temperature.

In our experiment, the voltage waveform is composed of three phases in each cycle: the spark discharge regime, the glow discharge regime, and the plasma off time. Each phase is associated with different electron densities and gas temperatures, so the chemical reactions that occur are likely also different. In addition, as noted above, the species created, heated, or excited in the current-carrying channel will diffuse to the near-room temperature region and react there as well.

We hypothesize the following primary mechanisms for reactive species generation in the spark-glow plasma. The spark phase is associated with the largest electron density and electron temperature [45] and promotes electron-impact reactions (reactions 4–6) and N_2^* quenching (reaction 7), generating a large number of O atoms. These O atoms react with N_2^* and N_2 and make NO (reaction 9 and 1). The spark phase is essential for forming larger amounts of NO (as demonstrated in figures 5 and 6).

The electron density and electron temperature of the glow discharge are considerably lower than in the spark phase, so production of O atom is reduced, leading to decreased production of NO via electron impact reactions [19–22, 45]. However, thermal reactions could be significant during this period. The primary chemical reaction of the glow discharge phase is hypothesized to be mostly reaction 14 because a greater glow percentage created a greater concentration of NO_2 according to our experimental results. The reaction of NO with ozone to form NO_2 (reaction 15) can also contribute to NO_2 formation, but the glow discharge phase has a relatively lower likelihood of containing ozone. The gas temperature in the glow discharge is relatively high (>2000 K) [19–22], which typically leads to thermal decomposition of O_3 (the reverse of reaction 8). Ozone is more likely formed in the spark phase and is immediately depleted by its reaction with NO (reaction 15). Indeed, no ozone was detected in the box by FTIR at any glow percentage, even during the first minute of the discharge operation.

The plasma off time does not create electrons by discharge, so the predominant reactions are collisions among remaining gas species. NO_x reduction occurs by reactions 11, 12, 13, and 16 in this phase. In summary, the formation of NO is the first step in forming NO_x, and the spark discharge is essential for NO formation. Maximizing the concentration of both NO and NO_2 requires maintaining a balance of the spark discharge and glow discharge phases.

Ambient air naturally contains water vapor, which also enters this complex NO_x formation chemistry. The key primary reaction is the electron-impact dissociation of H_2O forming H and OH radicals dominantly during the spark phase:

$$H_2O + e \rightarrow H + OH + e \quad (18)$$

Both H and OH react with NO and NO_2, leading to the formation of HNO_2 and HNO_3, which were also detected in the FTIR spectra. The presence of water vapor in the NO_x box also depletes NO_x, as demonstrated by the increase of aqueous nitrites and nitrates (figure 8) and so influences the gaseous NO_x chemistry. Investigations of water vapor concentration on the NO_x chemistry will be a subject of our future study.

It is beyond the scope of the present article to make a complete comparison with previous plasma-based bacterial inactivation results, but the present results are consistent with the rates and degrees of bacterial inactivation reported

previously [3, 8, 31, 46, 47]. Although it has apparently not been presented extensively in the scientific literature, recent commercial applications of gaseous NO_2 (generated by vaporizing liquid NO_2) as a room-temperature sterilization gas has clear relevance to the ideas and results presented in this article [48]. The concentrations apparently used in the commercial applications of NO_2 as a sterilization agent are also similar to those we have measured and report here. These recent reports of using NO_2 as a gaseous sterilizer for various surfaces (Noxilizer®) note rapid rates of bacterial spore inactivation (one log reduction in less than one minute) at NO_2 concentrations of about 2500–3000 ppm [48, 49]. Planktonic *E. coli* is generally much easier to inactivate than spores of spore-forming bacteria, and we achieved maximum disinfection after the gas phase concentration of NO_2 reached around 3000 ppm, suggesting that our gas mixtures were perhaps somewhat less potent. However, more detailed studies of the antimicrobial action of the gases created in the NO_x Box are needed in order to draw definitive conclusions.

There are many potential applications for the kind of plasma devices presented here. Plasma-activated water could be used for surface disinfection or even skin or wound antisepsis. Water treated by plasma contains high concentrations of nitrates and nitrites, and these compounds have been used for food preservation, especially for meats and fish, for many centuries. Nitrite has been extensively explored over the last 10–20 y, for various therapeutic applications, as has been summarized in recent reviews [28, 29]. Lundberg *et al* note that acidified nitrite has been shown to '…have potent antibacterial activity against a range of pathogens, including *Salmonella*, *Yersina* and *Shigella* species, *H. pylori*, and *Pseudomonas aerguinosa*' [28].

It must be acknowledged, of course, that safety issues are important when using plasma devices that create large concentrations of antimicrobial compounds that are also potentially highly toxic. The toxic compounds must be kept away from vulnerable individuals. In the case of NO_2, for example, chronic exposures can lead to various adverse health effects; the US EPA limits the 24 h exposure limit for NO_2 in outside air to 0.053 ppm [50]. Care must therefore be taken to ensure that risks for toxicity are minimized in whatever application is chosen for these plasma devices. One strategy under consideration and investigation is depleting toxic NO_2 gas in water, using a similar principle to the one used in industrial NO_x scrubbers. Therefore, the NO_x chemistry in the presence of water requires even further study.

5. Concluding remarks

We have shown that plasma devices based on spark-like air plasmas can efficiently produce strongly antimicrobial gas mixtures at rates that make them interesting for a variety of potential applications. The spark-like air plasma predominately creates NO_x mixtures that consist of about 90% NO_2 and 10% NO. Other major species detected include N_2O_4, HNO_2 and HNO_3. We demonstrated that either quasi-sinusoidal ac or square-wave dc waveforms will power automotive spark plugs to create these NO_x mixtures. Different sets of chemical reactions are associated with the spark and glow regimes of the discharge, and precise optimization of NO_x generation requires careful balancing of the spark and glow regimes. However, the ratio of NO to NO_2 in the volume varied only slightly with the degree of 'spark' to 'glow' character under the present conditions. NO is formed primarily in the initial transient spark regime and NO_2 forms later as NO is oxidized in various subsequent reactions. On a relative basis, NO is the first species to appear in the volume after initiating the discharge and when the plasma is extinguished, it disappears most rapidly. A discharge with predominantly, but not entirely, glow-like character appears to create the greatest concentration of NO_2 on the basis of the amount of energy expended. NO_2 appears to be the main antimicrobial compound created in the air spark-like plasma. Approximately 3000 ppm NO_2, created within the first 3 min of operation, is sufficient for rapid surface or water disinfection using *E. coli* as a model target microorganism.

The mechanisms of formation and loss of chemical species depend on both non-thermal electron-impact processes as well as thermal reactions. The fact that the plasma forms in a relatively narrow discharge channel means that there are large spatial gradients in charged and neutral species concentration as well as gas temperature. Furthermore, the presence of thermally induced gas convection in the closed volume, and inevitable surface reactions complicate any analysis of precise mechanisms responsible for the observed evolution in chemical species with time. However, the simplicity of the device design coupled with the growing realization that nitrogen oxides have many important biomedical applications suggests that air spark-like plasmas will receive increasing interest in the future.

Acknowledgments

The research was supported in part by the Department of Energy, Office of Fusion Science Plasma Science Center. Zdenko Machala's stay at UC Berkeley was supported by the Slovak-American Foundation. We acknowledge Alexander Lill (UC Santa Cruz) and Carly Anderson and Pritha Hait (UC Berkeley) for participating in some of the experiments. Takamasa Ichinao (formerly UC Berkeley visitor, now at Hitachi) contributed to the quantification of reactive species concentrations via HITRAN.

References

[1] De Geyter N and Morent R 2012 *Annu. Rev. Biomed. Eng.* **14** 255–74
[2] Rossi F, Moisan M, Kong M and Laroussi M 2012 *Plasma Process. Polym.* **9** 559–60
[3] Pavlovich M J, Chen Z, Sakiyama Y, Clark D S and Graves D B 2013 *Plasma Process. Polym.* **10** 69–76
[4] Klämpfl T G, Isbary G, Shimizu T, Li Y-F, Zimmermann J L, Stolz W, Schlegel J, Morfill G E and Schmidt H-U 2012 *Appl. Environ. Microbiol.* **78** 5077–82

[5] Weltmann K-D, Fricke K, Stieber M, Brandenburg R, von Woedtke T and Schnabel U 2012 *IEEE Trans. Plasma Sci.* **40** 2963–9
[6] Machala Z, Tarabova B, Hensel K, Spetlikova E, Sikurova L and Lukes P 2013 *Plasma Process. Polym.* **10** 649–59
[7] Pavlovich M J, Chang H-W, Sakiyama Y, Clark D S and Graves D B 2013 *J. Phys. D Appl. Phys.* **46** 145202
[8] Oehmigen K, Winter J, Hähnel M, Wilke C, Brandenburg R, Weltmann K-D and von Woedtke T 2011 *Plasma Process. Polym.* **8** 904–13
[9] Naïtali M, Herry J-M, Hnatiuc E, Kamgang G and Brisset J-L 2012 *Plasma Chem. Plasma Process.* **32** 675–92
[10] Brisset J-L and Hnatiuc E 2012 *Plasma Chem. Plasma Process.* **32** 655–74
[11] Robinson K M and Beckman J S 2005 *Methods Enzymol.* **396** 207–14
[12] Lukes P, Dolezalova E, Sisrova I and Clupek M 2014 *Plasma Sources Sci. Technol.* **23** 015019
[13] Babaeva N Y and Kushner M J 2013 *J. Phys. D Appl. Phys.* **46** 025401
[14] Sakiyama Y, Graves D B, Chang H-W, Shimizu T and Morfill G E 2012 *J. Phys. D Appl. Phys.* **45** 425201
[15] Bruggeman P J and Locke B R 2013 Assessment of potential applications of plasma with liquid water *Low Temperature Plasma Technology Methods and Applications* ed P K Chu and X P Lu (Boca Raton, FL: CRC) pp 367–400
[16] van Gils C a J, Hofmann S, Boekema B K H L, Brandenburg R and Bruggeman P J 2013 *J. Phys. D Appl. Phys.* **46** 175203
[17] Raizer Y 1997 *Gas Discharge Physics* (Berlin: Springer)
[18] Janda M and Machala Z 2011 *IEEE Trans. Plasma Sci.* **39** 2246–7
[19] Machala Z, Jedlovský I and Martisovits V 2008 *IEEE Trans. Plasma Sci.* **36** 918–9
[20] Yu L, Laux C O, Packan D M and Kruger C H 2002 *J. Appl. Phys.* **91** 2678
[21] Machala Z, Marode E, Laux C and Kruger C H 2004 *J. Adv. Oxid. Technol.* **7** 133–7
[22] Machala Z, Janda M, Hensel K, Jedlovský I, Leštinská L, Foltin V, Martišovitš V and Morvová M 2007 *J. Mol. Spectrosc.* **243** 194–201
[23] Maly R R 2009 *Flow and Combustion in Reciprocating Engines* (Berlin: Springer)
[24] Halliwell B and Gutteridge J 2007 *Free Radicals in Biology and Medicine* (New York: Oxford University)
[25] Bogdan C 2001 *Trends Cell Biol.* **11** 66–75
[26] Graves D B 2012 *J. Phys. D. Appl. Phys.* **45** 263001
[27] Seinfeld J H and Pandis S 2006 *Atmospheric Chemistry and Physics: From Air Pollution to Climate Change* (New York: Wiley)
[28] Lundberg J O, Weitzberg E and Gladwin M T 2008 *Nat. Rev. Drug Discov.* **7** 156–67
[29] Vitturi D a and Patel R P 2011 *Free Radic. Biol. Med.* **51** 805–12
[30] Fridman A 2008 *Plasma Chemistry* (Cambridge: Cambridge University Press)
[31] Traylor M J, Pavlovich M J, Karim S, Hait P, Sakiyama Y, Clark D S and Graves D B 2011 *J. Phys. D Appl. Phys.* **44** 472001
[32] Pavlovich M J, Clark D S and Graves D B 2014 *Plasma Sources Sci. Technol.* **23** 065036
[33] Vasilets V N and Shekhter A B 2012 *Plasma Bio-Decontamination, Medicine and Food Security* (Berlin: Springer)
[34] Dobrynin D, Arjunan K, Fridman a, Friedman G and Clyne a M 2011 *J. Phys. D Appl. Phys.* **44** 075201
[35] Kim T, Song S, Kim J and Iwasaki R 2010 *Japan. J. Appl. Phys.* **49** 126201
[36] Snyder R and Hisatsune I 1957 *J. Chem. Phys.* **624** 960–2
[37] Melen F, Pokorni F and Herman M 1992 *Chem. Phys. Lett.* **194** 181–6
[38] Ahro M and Kauppinen J 2001 *Appl. Spectrosc.* **55** 50–4
[39] Hnatiuc B, Astanei D, Pellerin S, Cerqueira N and Hnatiuc M 2014 *Contrib. Plasma Phys.* **54** 712–23
[40] Oliveira C, Reis J, Souza-Corrêa J, Dal Pino A and Amorim J 2012 *J. Phys. D Appl. Phys.* **45** 255201
[41] Miller J and Bowman C 1989 *Prog. Energy Combust. Sci.* **15** 287–338
[42] Ivanov M, Kiverin A, Klumov B and Fortov V 2014 *Phys.—Usp.* **57** 234–49
[43] Sakai S, Matsuda M, Wang D, Namihira T, Akiyama H, Okamoto K and Toda K 2009 *Acta Phys. Pol. A* **115** 1104–6
[44] Kossyi I, Kostinsky A, Matveyev A and Silakov V 1992 *Plasma Sources Sci. Technol.* **1** 207–20
[45] Janda M, Martišovitš V, Hensel K, Dvonc L and Machala Z 2014 *Plasma Sources Sci. Technol.* **23** 065016
[46] Kamgang-Youbi G, Herry J-M, Meylheuc T, Brisset J-L, Bellon-Fontaine M-N, Doubla A and Naïtali M 2009 *Lett. Appl. Microbiol.* **48** 13–8
[47] Oehmigen K, Hähnel M, Brandenburg R, Wilke C, Weltmann K-D and von Woedtke T 2010 *Plasma Process. Polym.* **7** 250–7
[48] Kulla J, Reich R and Broedel S Jr 2009 Sterilizing combination products using oxides of nitrogen *Medical Device and Diagnostic Industry* www.mddionline.com/print/2289
[49] Carbone P, Benedek K, Ruffo M and Luongo W 2013 Device and method for gas sterilization *US Patent 2013/0230430A1*
[50] United States Environmental Protection Agency 2012 An introduction to indoor air quality (IAQ): nitrogen dioxide (NO_2) (www.epa.gov/iaq/no2.html)